Journal of the Brazilian Society of Mechanical Sciences and Engineering (2020) 42:19
https://doi.org/10.1007/s40430-019-2103-2

TECHNICAL PAPER

A theoretical nanofluid analysis exhibiting hydromagnetics characteristics employing CVFEM

S. Mondal[1] · A. S. Dogonchi[2] · N. Tripathi[3] · M. Waqas[4] · Seyyed Masoud Seyyedi[2] · M. Hashemi-Tilehnoee[2] · D. D. Ganji[5]

Received: 25 March 2019 / Accepted: 8 November 2019 / Published online: 3 December 2019

Abstract
The heat transfer properties of current liquids are specifically improved by suspending nanocrystalline solid elements smaller than 100 nm in diameter. These liquids are considered as potential working fluids for applications such as car radiators, solar collectors, electronic frost systems, nuclear reactors and heat pipes. Due to such uses, here we formulate CuO–H_2O nanofluids in a two-dimensional circular geometry with a rhombus-shaped barrier maintaining the constant temperature of two adjacent high walls. The streamlines and isotherms have been plotted using the control volume finite element method and applying the KKL model for nanofluid simulation. The results were calculated for different concentrations of nanoparticles, Hartmann number and Rayleigh number. It was found that in a large number of volume fraction and Hartmann number, the isotherms near the outer margin are more prominent while the low-volume-concentration isotherms are concentrated near the adiabatic wall of the obstacle. It was also found that there is a temperature gradient in the radial direction at a higher volume fraction and Hartmann number (Ha). The temperature gradient was limited to adiabatic walls of the obstruction in lower volume fraction and Ha. Two similar shapes but differently directed eddies are formed for any value of Ra in streamlines. $|\Psi_{max}|_{nf}$ increases with an increase in the values of Ra from 10^3 to 10^5.

Keywords Nanofluid · Natural convection · Magnetic field · CVFEM · KKL

1 Introduction

Nowadays, the major need for modern technological industries is high-performance cooling for standard production. By the submersion of nanoparticles to the base fluid, high-performance cooling can be achieved. The major drawbacks of conventional fluids in heat transfer processes are due to the lack of proper thermal conductivity. Nanofluids can overcome this problem. One of the important applications of nanofluid in thermal sciences was developed by Eastman et al. [1]. They pioneered the idea of using nanoparticles in thermal engineering. An important role of heat transfer in most industrial applications is to dissipate heat to the surroundings from the high-temperature surfaces of different devices. Hence, convection plays a major role to dissipate this heat. Free or natural convection is caused primarily due to the temperature difference between different surfaces [2]. Many investigations have been published so far to improve the free convection heat transfer such as changing the flow surface geometry, altering the boundary values, using additives in fluids, using extended surfaces and application of different external forces

Technical Editor: Erick de Moraes Franklin, Ph.D.

✉ A. S. Dogonchi
sattar.dogonchi@yahoo.com

✉ M. Waqas
mw_qau88@yahoo.com

1 Department of Mathematics, Amity University, Kolkata, Newtown, West Bengal 700135, India

2 Department of Mechanical Engineering, Aliabad Katoul Branch, Islamic Azad University, Aliabad Katoul, Iran

3 Department of Mechanical Engineering, Amity University, Kolkata, Newtown, West Bengal 700135, India

4 NUTECH School of Applied Sciences and Humanities, National University of Technology, Islamabad 44000, Pakistan

5 Mechanical Engineering Department, Babol Noshirvani University of Technology, Babol, Iran

in the surface geometry [2]. A lot of computational studies have been carried out in different geometries using different nanofluids. Tiwari and Das [3] studied a two-sided lid-driven differentially heated square cavity to analyse the behaviour of Cu–water nanofluid using SIMPLE algorithm finite volume approach. Adjacent two walls were moving at a constant temperature, while the other two walls were insulated. It was concluded that the Richardson Number and the direction of the fluid flow affect the heat transfer and fluid flow. Iwatsu et al. [4] investigated a square cavity with a temperature gradient between the top and bottom walls having a viscous fluid. Numerical analysis was performed to predict the thermal and velocity fields. The results showed that the heat transfer was intensified when $Gr/Re^2 \ll 1$. Sharifpur et al. [5] investigated the heat transfer in a rectangular cavity filled by ethylene glycol (EG)–water as the nanofluid. Two walls were externally heated, and the analysis was performed using ANSYS Fluent 15 to predict the local Nusselt number distribution. Koo et al. [6–8] studied the impact of different micro-scale parameters such as surface roughness on the heat transfer of micro-heat sink systems. Dogonchi et al. [9, 10] investigated the influence of Brownian motion on the thermal conductivity of nanofluids in non-parallel stretching walls. They concluded that the velocity, temperature, Nusselt number boosts with increase in stretching parameter. They also considered the effects of the magnetic parameter, volume fraction and radiation parameter of the nanofluid on velocity and temperature profiles. Mastianiet al. [11] studied Cu–water-based nanofluid in a laminar mixed convection flow for different lid-driven cavities. They had taken different volume fractions for both Boussinesq and non-Boussinesq approximations to analyse the streamlines, isotherms, mid-plane velocities, mid-plane temperature and the average Nusselt (Nu) number in different boundary conditions. It was concluded that the Nu number increases as the volume fraction of the nanoparticles grows. The effect of buoyancy forces and shear forces on the Nusselt number had also been studied. Mahapatra et al. [12] studied the effect of the magnetic field in a two-dimensional natural convection flow in an inclined enclosure. They considered the effect of thermal radiation and heat generation on the flow pattern and temperature field. In the present study, we are trying to focus on natural convection nanofluid flow in an annulus between a circular cylinder and a rhombus enclosure. The novelty of the modelled problem is based on the following aspects.

1. Natural convective nanofluid flows in an annulus between a circular cylinder and a rhombus enclosure is scrutinized.
2. Hydromagnetics characteristics are addressed firstly in this communication.
3. Computations are carried out through the novel CVFEM approach.

2 Problem description and basic equations

CuO–water nanofluid natural convection in an annulus between a circular cylinder and a rhombus enclosure under magnetic field is investigated (Fig. 1). The continuity, momentum and energy equations for two-dimensional steady-state natural convection flow in the enclosure can be defined as:

$$\frac{\partial u}{\partial x} + \frac{\partial v}{\partial y} = 0 \tag{1}$$

$$\rho_{\mathrm{nf}}\left(u\frac{\partial u}{\partial x} + v\frac{\partial u}{\partial y}\right) = -\frac{\partial p}{\partial x} + \mu_{\mathrm{nf}}\left(\frac{\partial^2 u}{\partial x^2} + \frac{\partial^2 u}{\partial y^2}\right) + \sigma_{\mathrm{nf}}\left(B_y B_x v - B_y^2 u\right) \tag{2}$$

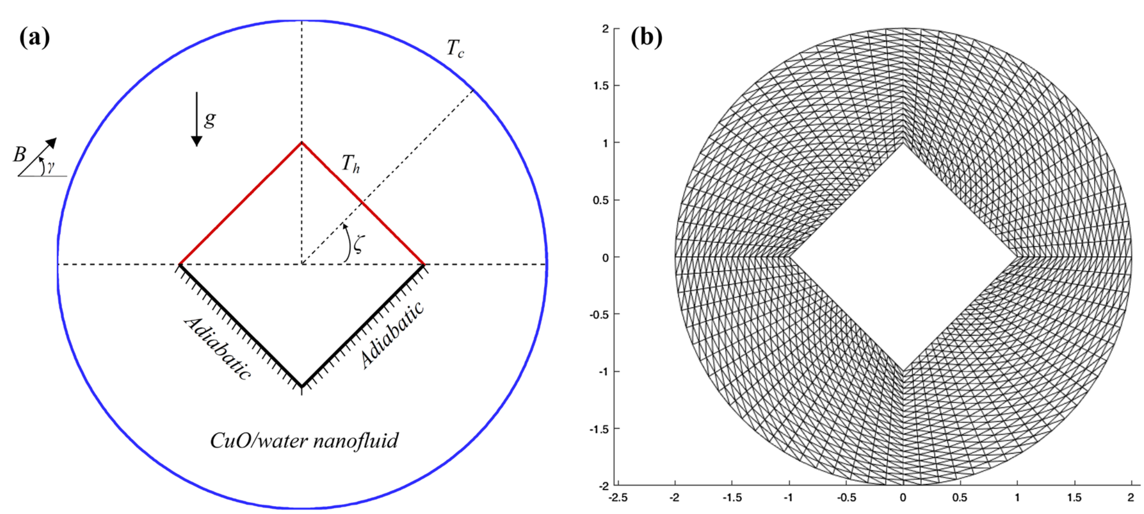

Fig. 1 **a** Physical model and coordinate system **b** grid distribution

$$\rho_{\mathrm{nf}}\left(u\frac{\partial v}{\partial x}+v\frac{\partial v}{\partial y}\right)=-\frac{\partial p}{\partial y}+\mu_{\mathrm{nf}}\left(\frac{\partial^2 v}{\partial x^2}+\frac{\partial^2 v}{\partial y^2}\right)+\rho_{\mathrm{nf}}\beta_{\mathrm{nf}}g\left(T-T_{\mathrm{c}}\right)+\sigma_{\mathrm{nf}}\left(B_yB_xu-B_x^2v\right) \tag{3}$$

$$u\frac{\partial T}{\partial x}+v\frac{\partial T}{\partial y}=\frac{k_{\mathrm{nf}}}{\left(\rho C_p\right)_{\mathrm{nf}}}\left(\frac{\partial^2 T}{\partial x^2}+\frac{\partial^2 T}{\partial y^2}\right) \tag{4}$$

where $B_x=B_0\cos\gamma$, $B_y=B_0\sin\gamma$.

ρ_{nf}, $(\rho Cp)_{\mathrm{nf}}$, $(\rho\beta)_{\mathrm{nf}}$ and σ_{nf} are defined as follows:

$$\rho_{\mathrm{nf}}=(1-\phi)\rho_{\mathrm{f}}+\phi\rho_{\mathrm{s}} \tag{5}$$

$$\left(\rho C_{\mathrm{p}}\right)_{\mathrm{nf}}=(1-\phi)\left(\rho C_{\mathrm{p}}\right)_{\mathrm{f}}+\phi\left(\rho C_{\mathrm{p}}\right)_{\mathrm{s}} \tag{6}$$

$$(\rho\beta)_{\mathrm{nf}}=(1-\phi)(\rho\beta)_{\mathrm{f}}+\phi(\rho\beta)_{\mathrm{s}} \tag{7}$$

$$\frac{\sigma_{\mathrm{nf}}}{\sigma_{\mathrm{f}}}=1+\frac{3\left(\frac{\sigma_{\mathrm{s}}}{\sigma_{\mathrm{f}}}-1\right)\phi}{\left(\frac{\sigma_{\mathrm{s}}}{\sigma_{\mathrm{f}}}+2\right)-\left(\frac{\sigma_{\mathrm{s}}}{\sigma_{\mathrm{f}}}-1\right)\phi} \tag{8}$$

The KKL (Koo–Kleinstreuer–Li) correlations for k_{nf} and μ_{nf} by taking into account the Brownian motion are as [6–10]:

$$k_{\mathrm{nf}}=k_{\mathrm{static}}+k_{\mathrm{Brownian}} \tag{9}$$

$$\mu_{\mathrm{nf}}=\mu_{\mathrm{static}}+\mu_{\mathrm{Brownian}}=\mu_{\mathrm{static}}+\frac{k_{\mathrm{Brownian}}}{k_{\mathrm{f}}}\times\frac{\mu_{\mathrm{f}}}{\mathrm{Pr}} \tag{10}$$

In which

$$\frac{k_{\mathrm{static}}}{k_{\mathrm{f}}}=\frac{k_{\mathrm{s}}+(m-1)k_{\mathrm{f}}-(m-1)\phi\left(k_{\mathrm{f}}-k_{\mathrm{s}}\right)}{k_{\mathrm{s}}+(m-1)k_{\mathrm{f}}+\phi\left(k_{\mathrm{f}}-k_{\mathrm{s}}\right)} \tag{11}$$

$$\mu_{\mathrm{static}}=\frac{\mu_{\mathrm{f}}}{(1-\phi)^{2.5}} \tag{12}$$

$$k_{\mathrm{Brownian}}=5\times10^4\phi\left(\rho C_{\mathrm{p}}\right)_{\mathrm{f}}\sqrt{\frac{k_{\mathrm{b}}T}{\rho_{\mathrm{s}}d_{\mathrm{s}}}}\beta'\left(T,\phi,d_{\mathrm{s}}\right) \tag{13}$$

Here, m is the shape factor. The shape factor for various particle shapes is given in Table 1 [13–15]. In addition, the nanofluid thermo-physical features are portrayed in Table 2 [16–18].

In Eq. (14), the empirical β'-function is defined as follows:

Table 1 Shape factor values for various nanoparticle shapes [13–15]

Particle shapes	Spherical	Cylinder	Platelet
			
m	3	4.8	5.7

$$\beta'\left(T,\phi,d_{\mathrm{s}}\right)=\left(a_1+a_2\ln\left(d_{\mathrm{s}}\right)+a_3\ln(\phi)+a_4\ln(\phi)\ln\left(d_{\mathrm{s}}\right)+a_5\ln\left(d_{\mathrm{s}}\right)^2\right)\ln(T)+\left(a_6+a_7\ln\left(d_{\mathrm{s}}\right)+a_8\ln(\phi)+a_9\ln(\phi)\ln\left(d_{\mathrm{s}}\right)+a_{10}\ln\left(d_{\mathrm{s}}\right)^2\right) \tag{14}$$

where the coefficients a_i $(i=0.0.10)$ for CuO-H_2O nanofluid are portrayed in Table 3.

The vorticity and stream function are defined as follows:

$$v=-\frac{\partial\psi}{\partial x},\quad u=\frac{\partial\psi}{\partial y},\quad \omega=\frac{\partial v}{\partial x}-\frac{\partial u}{\partial y} \tag{15}$$

We define these dimensionless variables:

$$X=\frac{x}{L},\ Y=\frac{y}{L},\ \Pi=\frac{\omega L^2}{\alpha_{\mathrm{f}}},\ \Psi=\frac{\psi}{\alpha_f},\quad U=\frac{uL}{\alpha_{\mathrm{f}}},\ V=\frac{vL}{\alpha_{\mathrm{f}}},\ \theta=\frac{T-T_{\mathrm{c}}}{T_{\mathrm{h}}-T_{\mathrm{c}}} \tag{16}$$

Considering Eq. (16), the governing equations change to following form:

$$\frac{\partial\Psi}{\partial Y}\frac{\partial\Pi}{\partial X}-\frac{\partial\Psi}{\partial X}\frac{\partial\Pi}{\partial Y}=\frac{\mu_{\mathrm{nf}}/\mu_{\mathrm{f}}}{\rho_{\mathrm{nf}}/\rho_{\mathrm{f}}}\mathrm{Pr}\left(\frac{\partial^2\Pi}{\partial X^2}+\frac{\partial^2\Pi}{\partial Y^2}\right)+\frac{\beta_{\mathrm{nf}}}{\beta_{\mathrm{f}}}\mathrm{Ra}\,\mathrm{Pr}\,\frac{\partial\theta}{\partial X}+\frac{\sigma_{\mathrm{nf}}/\sigma_{\mathrm{f}}}{\rho_{\mathrm{nf}}/\rho_{\mathrm{f}}}\mathrm{Ha}^2\,\mathrm{Pr}\left(B_y'^2\frac{\partial U}{\partial Y}+B_x'B_y'\frac{\partial U}{\partial X}-B_x'^2\frac{\partial V}{\partial X}-B_x'B_y'\frac{\partial V}{\partial Y}\right) \tag{17}$$

$$\frac{\partial\Psi}{\partial Y}\frac{\partial\theta}{\partial X}-\frac{\partial\Psi}{\partial X}\frac{\partial\theta}{\partial Y}=\frac{k_{nf}/k_f}{\left(\rho C_p\right)_{nf}/\left(\rho C_p\right)_f}\left(\frac{\partial^2\theta}{\partial X^2}+\frac{\partial^2\theta}{\partial Y^2}\right) \tag{18}$$

$$\frac{\partial^2\Psi}{\partial X^2}+\frac{\partial^2\Psi}{\partial Y^2}=-\Pi \tag{19}$$

Subject to the boundary conditions:

$$\begin{aligned}&\theta=1 && \text{on the local heater}\\&\theta=0 && \text{on the outer circular wall}\\&\Psi=0 && \text{on the all walls}\end{aligned} \tag{20}$$

where $\mathrm{Pr}=\nu_{\mathrm{f}}/\alpha_{\mathrm{f}}$ is the Prandtl number, $\mathrm{Ra}=g\beta_{\mathrm{f}}\left(T_{\mathrm{h}}-T_{\mathrm{c}}\right)L^3/\alpha_{\mathrm{f}}\nu_{\mathrm{f}}$ is the Rayleigh number and $\mathrm{Ha}=B_0L\sqrt{\sigma_{\mathrm{f}}/\mu_{\mathrm{f}}}$ is the Hartmann number.

The local and average Nusselt numbers along the cold wall can be defined as:

Table 2 Thermo-physical features of nanoparticle and water [16–18]

	ρ (kg/m^3)	C_p (J/kg K)	k (W/m K)	$\beta \times 10^5$ (K^{-1})	σ ((Ωm)$^{-1}$)	dp (nm)
CuO	6500	540	18	1.8	2.7×10^{-8}	29
Pure water	997.1	4179	0.613	21	0.05	–

Table 3 The coefficient values of CuO–water nanofluid [9, 10]

Coefficient values	CuO–water
a_1	−26.59331085
a_2	−0.403818333
a_3	−33.3516805
a_4	−1.915825591
a_5	6.42185846658E−02
a_6	48.40336955
a_7	−9.787756683
a_8	190.24561
a_9	10.92853866
a_{10}	−0.720099837

Table 4 Comparison between present results and other works for the average Nusselt number (Nu_{avg})

Ra	Present work	Khanafer et al. [25]	De Vahl Davis [26]
10^3	1.1307	1.118	1.118
10^4	2.2674	2.245	2.243
10^5	4.5851	4.522	4.519
10^6	8.8341	8.826	8.799

$$\mathrm{Nu}_{\mathrm{loc.}} = -\frac{k_{\mathrm{nf}}}{k_{\mathrm{f}}}\frac{\partial\theta}{\partial n} \tag{21}$$

$$\mathrm{Nu}_{\mathrm{ave.}} = \frac{1}{2\pi}\int_0^{2\pi} \mathrm{Nu}_{\mathrm{loc.}} \mathrm{d}\zeta \tag{22}$$

where n is the direction normal to the outer walls.

3 Numerical solution and validation

Here, the governing equations of this new type of mathematical model are solved via the control volume finite element method (CVFEM) [19–24]. Table 4 shows the comparison between present results and other works for the average Nusselt number (Nu_{avg}). The results in this table show good agreement with previously published results. To attain mesh independence, various mesh sizes are examined (see Table 5). It is found that the grid of 41×431 must be chosen for the present problem.

Table 5 Influence of grid size on Nu_{avg} when $Ra=10^5$, $Ha=50$ and $m=3$

Grid dimension	Nu_{avg}
21 × 211	0.914310
31 × 321	0.952095
41 × 431	0.973970
51 × 541	0.978744

4 Results and discussion

Figures 2, 3 and 4 display the effect of Ha on streamlines and isotherms for different values of Ra from 10^3 to 10^5 when the volume fraction of the nanofluid (ϕ) is zero and shape factor of nanoparticles (m) is 3. Figure 2 describes the streamlines and isotherms for different Ra in accordance with the Ha = 0. Two similar shapes of eddies are formed for any value of Ra within this range, but the directions of the streamlines for different eddies are different. Clockwise and anticlockwise flows are shown via negative and positive signs of stream functions, respectively. Again, it can be shown that by increasing Rayleigh number from 10^3 to 10^5, the modulus values of the different directed eddies at the centre will increase. So, the $|\Psi_{max}|_{nf}$ increases with increase in the values of Ra from 10^3 to 10^5. Moreover, the Ra is substantially higher the circular eddies are disturbed and streamlines are more predominant in the outer circular periphery. With higher $|\Psi_{max}|_{nf}$, Ra increases and the nature of streamlines is perturbed. The decreasing nature of the heat transfer gradient is observed with higher $|\Psi_{max}|_{nf}$. At lower $|\Psi_{max}|_{nf}$, the isotherms are concentrated near the heated obstacles walls, whereas at higher $|\Psi_{max}|_{nf}$ the isotherms are dispersed from the heated walls to the outer circular periphery walls.

In Fig. 3, the streamlines and isotherms are depicted for different values of Ra from 10^3 to 10^5 when Ha = 25. The streamlines are observed to be more circular by increasing the fluid velocity. Eddies formed are smaller with higher values of Ra. When the Ra is low, the isotherms are formed near the boundary of the heated obstacle surfaces. With the increase in Ra, the isotherms diverge towards the outer circular periphery. The temperature gradient is

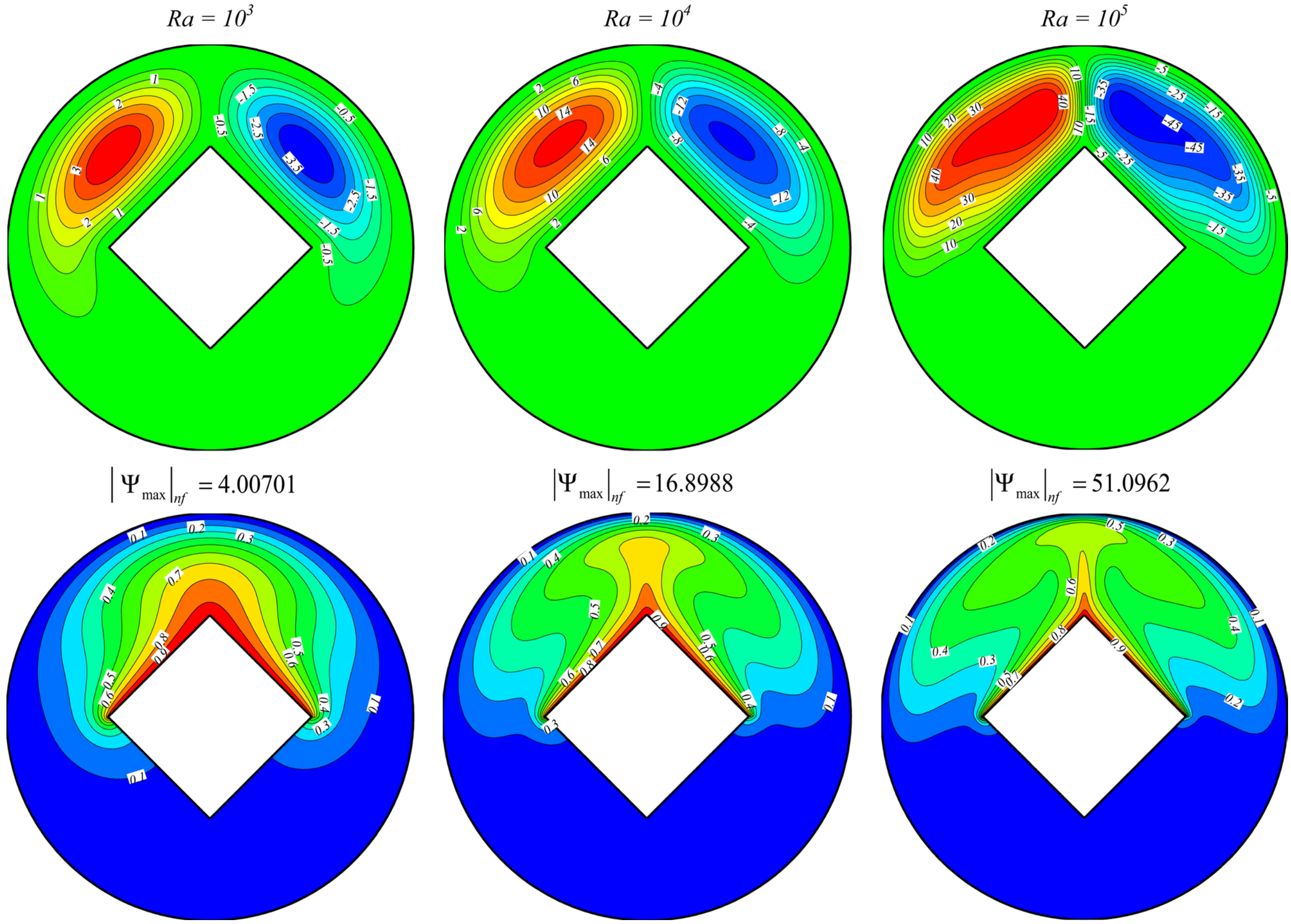

Fig. 2 Streamlines and isotherms for different values of Ra when Ha = 0, ϕ = 2% and m = 3

higher at the edge boundaries and decreases thereafter in the radial direction at lower values of Ra. The other nature of streamlines and isotherms is same, as shown in Fig. 2. Figure 4 describes the streamlines and isotherms when the Ha is further increased to 50 for the same range of Ra. From this figure, it can be seen that with increasing Ra, the circular nature of streamlines is more predominating. So, the streamlines are more concentrated for the increasing value of Ra. The other nature of streamlines and isotherms is similar, as shown in Fig. 2.

Figure 5 shows the comparison of streamlines and isotherms of various nanofluids for different ϕ and Ra when Ha = 25, m = 3. By decreasing the Rayleigh number from 10^5 to 10^3, the streamlines are more dispersed. This effect is more predominant while the volume fraction is further increased. Thereby, $|\Psi_{max}|_{nf}$ value increases with the increase in the volume fraction for each value of Ra. Also when the volume fractions are fixed, and the Ra is increased from 10^3 to 10^5, there is a considerable increase in $|\Psi_{max}|_{nf}$. When Ra = 10^3, the isotherms are observed near all the four obstacle walls. The temperature gradient is also uniform. But with the increase in Ra, this nature diminishes. The isotherms are concentrated more towards the outer periphery from the heated wall.

Figure 6 displays the dependency of local Nusselt number (Nu_{loc}) with different values of Ha, Ra and ϕ. At Ra = 10^3 and Ha = 25, the Nu_{loc} increases with increase in the ϕ up to a certain range of ζ, after which the same nature is observed with decreasing value of Nu_{loc} and the same patterns are observed again forming a sinusoidal curve. But when Ha = 50, the maximum values of Nu_{loc} are lesser than the maximum values of Nu_{loc} when Ha = 25 for any value of ϕ. Other nature of Nu_{loc} remains unchanged. This shows that the increasing value of Ha decreases the heat transfer rate of the nanofluid. Again, there will be no such changes in Nu_{loc} for the increasing value of ϕ when Ra = 10^4 and Ha = 25. But as ζ boosts up to a certain range, Nu_{loc} forms a pick for any value of ϕ. But, when Ha = 50, Nu_{loc} grows with the decreasing value of ϕ and it coincides at a point with forming a pick for the lower value of ζ. For a higher value of ζ, the curve pattern of Nu_{loc} is same as we described before but the maximum value of Nu_{loc} is less compared to the higher

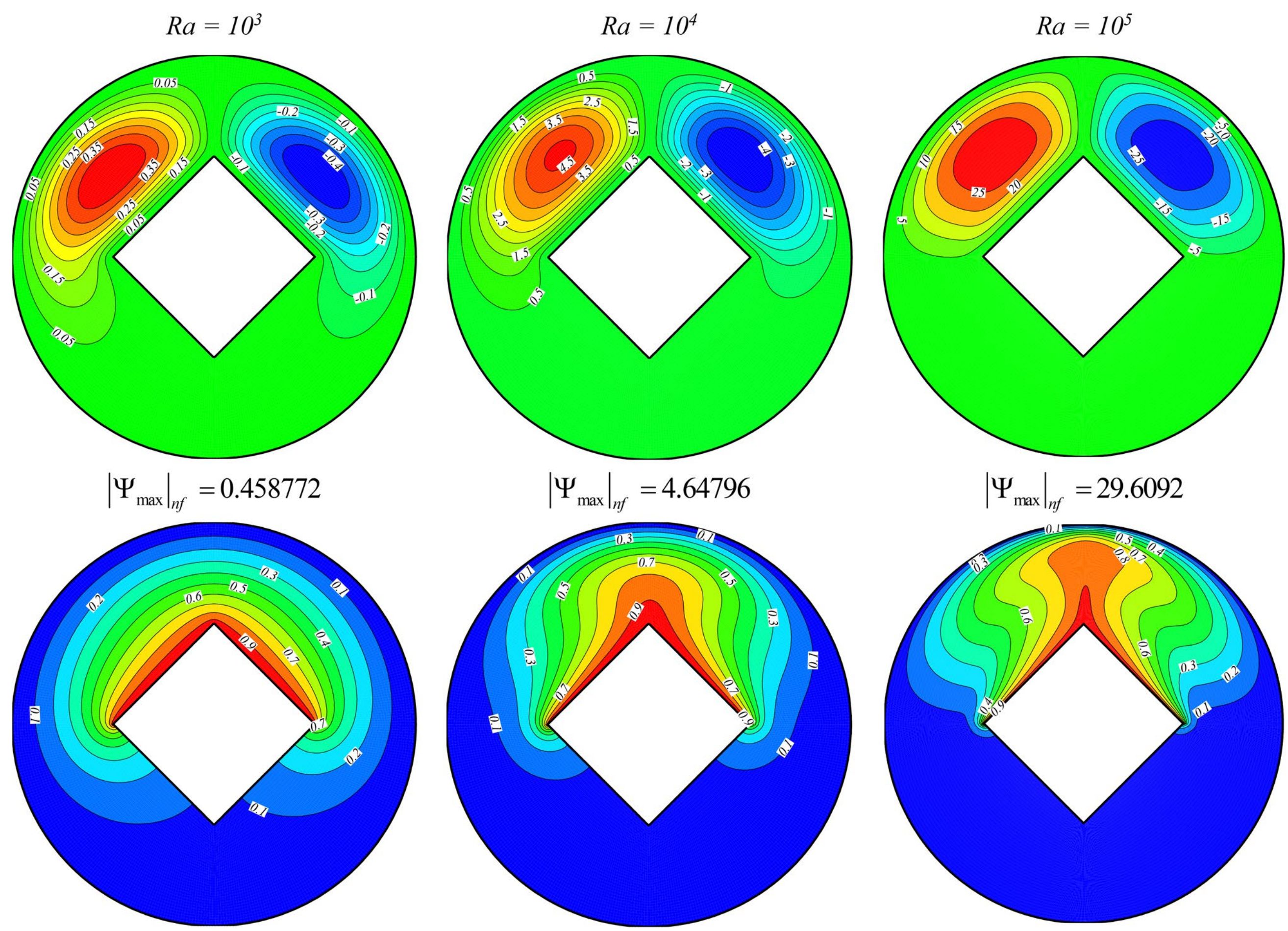

Fig. 3 Streamlines and isotherms for different values of Ra when Ha = 25, ϕ = 2% and m = 3

value of Ha. When Ra = 10^5 and Ha = 25, the $\mathrm{Nu}_{\mathrm{loc}}$ remains unchanged for any value of ϕ, but as it reaches a pick, different values are found for different ϕ. When Ha = 50, the $\mathrm{Nu}_{\mathrm{loc}}$ is slightly different only at a pick with a different value of ϕ. From Fig. 6, it can be concluded that the $\mathrm{Nu}_{\mathrm{loc}}$ lessens with increasing values of Ra for any value of Ha. Also, it can be seen that the lowest value of $\mathrm{Nu}_{\mathrm{loc}}$ occurs within a short range of $\zeta = 270°$. From Fig. 7, it is obvious that by increasing the nanoparticle shape factor the $\mathrm{Nu}_{\mathrm{loc}}$ also goes up for the fixed value of Ra, Ha and $\phi = 2\%$ when $\mathrm{Nu}_{\mathrm{loc}}$ maintaining the same pattern of heat transfer rate, as shown in Fig. 6 for specific Ra and Ha. From Fig. 7, it is seen that by increasing Rayleigh number $\mathrm{Nu}_{\mathrm{loc}}$ augments for a fixed value of Ha when $\phi = 2\%$. In addition, it can be seen that the lowest value of $\mathrm{Nu}_{\mathrm{loc}}$ occurs within a short range of $\zeta = 270°$.

Figure 8 depicts the average Nusselt number ($\mathrm{Nu}_{\mathrm{ave}}$) for different values of Ra, Ha and ϕ when $m = 3$. From this figure, it can be seen that $\mathrm{Nu}_{\mathrm{ave}}$ is decreasing with the increasing value of ϕ from 2 to 4% for any fixed value of Ra and Ha. Also $\mathrm{Nu}_{\mathrm{ave}}$ enhances with an increase in the value of Ra from 10^3 to 10^5 for the fixed value of Ha and ϕ. For the fixed value of Ra and ϕ, $\mathrm{Nu}_{\mathrm{ave}}$ is maximum when Ha boosts. Figure 9 shows the $\mathrm{Nu}_{\mathrm{ave}}$ with respect to the different values of Ra, Ha and m when $\phi = 2\%$. Increasing nanoparticle shaping factor increases $\mathrm{Nu}_{\mathrm{ave}}$ for any fixed value of Ha and Ra. Similarly, with an increase in Ra, $\mathrm{Nu}_{\mathrm{ave}}$ also grows for any fixed value of Ha and m. It can be also seen that $\mathrm{Nu}_{\mathrm{ave}}$ rapidly increases within the range of 10^4 and 10^5. Also by increasing Hartmann number, the maximum $\mathrm{Nu}_{\mathrm{ave}}$ diminishes for any fixed value of m and Ra.

At high Ha and low Ra, average Nu has a lesser gradient, which implies that it grows at a lower rate with an increment in Ra at high Ha. But at low Ra number and low Ha, Nu boosts at a higher proportion as compared to the former. This concludes that average Nu has an inverse relation with Ha at low Ra, but at higher Ra, the average Nu relationship with Ha is not maintained.

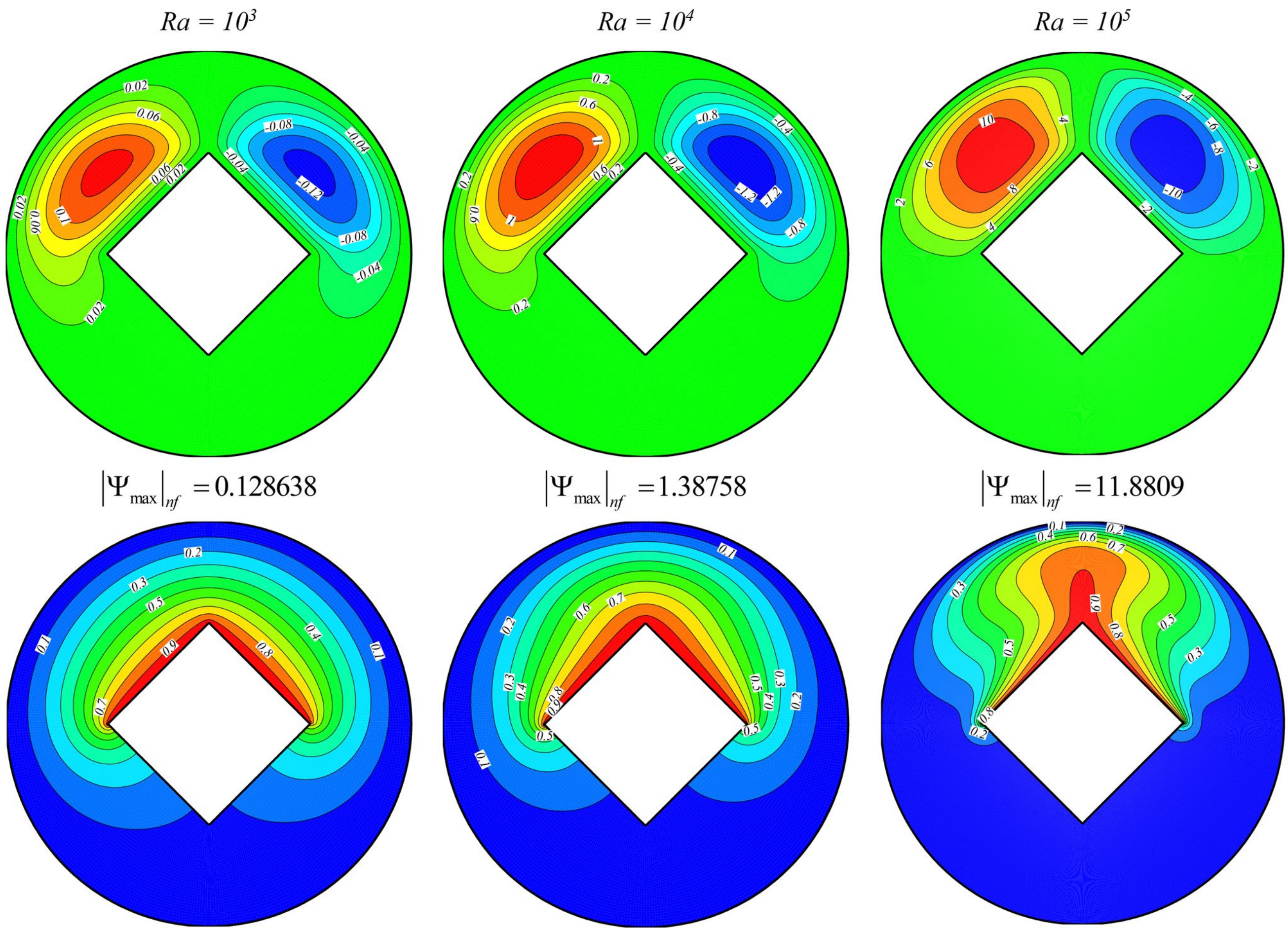

Fig. 4 Streamlines and isotherms for different values of Ra when Ha = 50, $\phi = 2\%$ and $m = 3$

5 Conclusions

CuO–water nanofluid is taken in a 2D circular geometry with a rhombus-shaped obstacle maintaining a constant temperature of the upper two adjacent walls. The streamlines and isotherms have been resulted using the control volume finite element method by applying KKL model for the simulation of nanofluid. Two similar shapes but differently directed eddies are formed for any value of Ra in streamlines. Again, $|\Psi_{max}|_{nf}$ increases with an increase in the values of Ra from 10^3 to 10^5. The results have confirmed that isotherms were concentrated at the adiabatic obstacle walls at a low value of the Rayleigh number in the nanofluid flow, and also the temperature gradient was less in the radial direction in this same condition. It can be concluded that the heat transfer is affected for a low value of Rayleigh number. Similarly, eddies are formed near the adiabatic walls of the obstacle for low value of Rayleigh number. By increasing the volume fraction of the nanoparticles, more eddies are formed and also it diverges near the outer periphery.

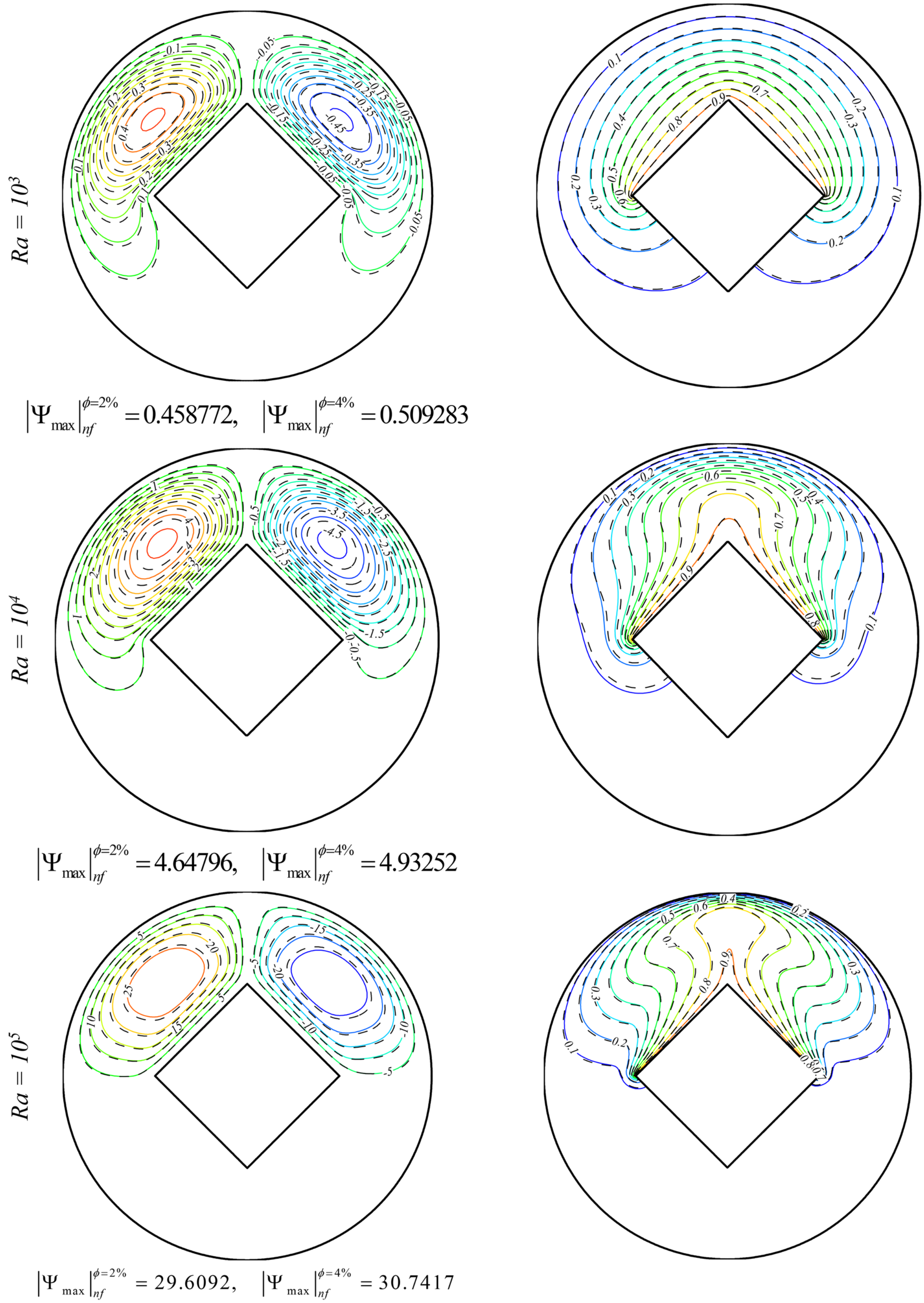

Fig. 5 Comparison of the streamlines and isotherms between various nanofluids (dashed lines—ϕ = 4% and solid lines—ϕ = 2%) for different values of Ra when Ha = 25 and m = 3

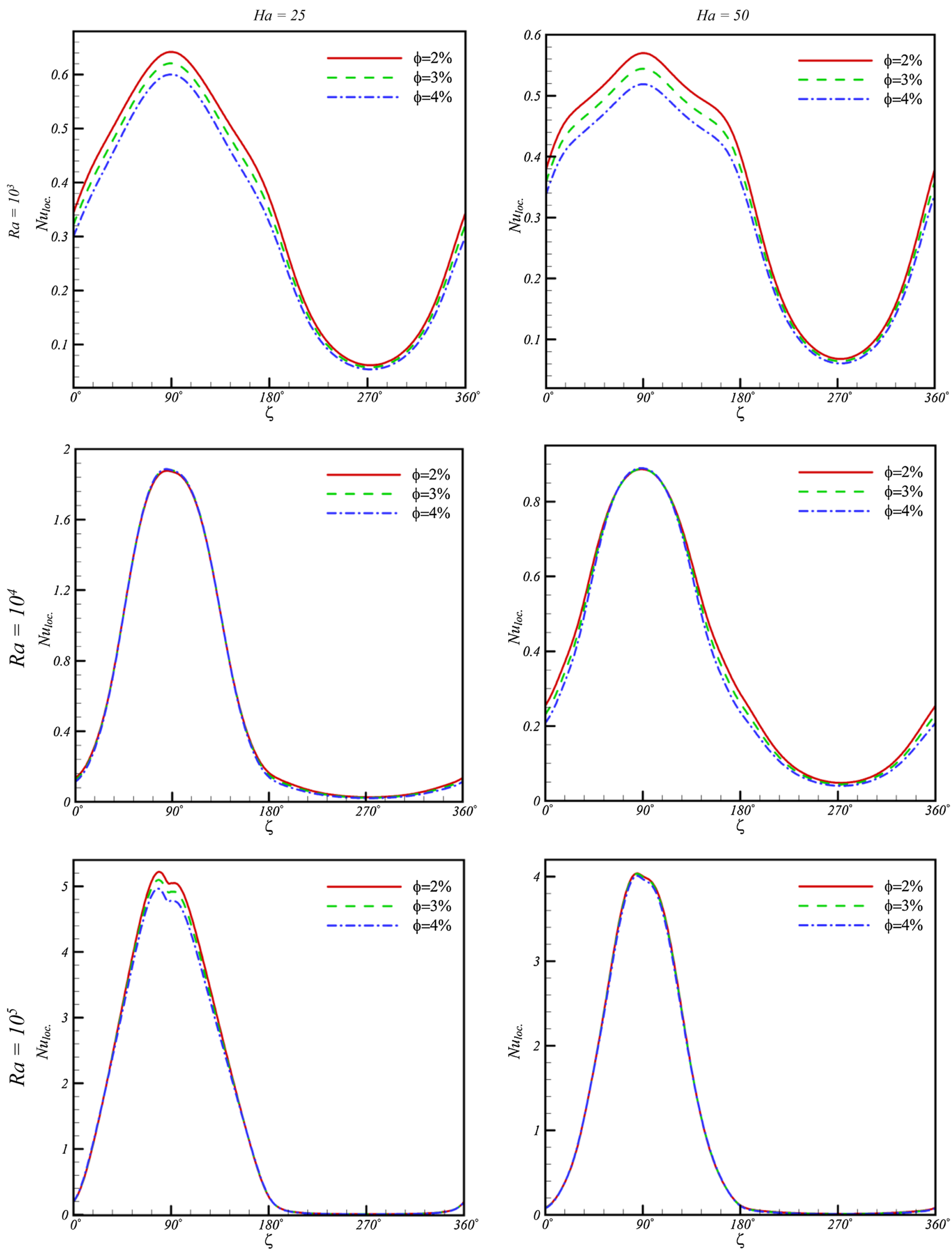

Fig. 6 Local Nusselt number ($Nu_{loc.}$) for different values of Ra, Ha and ϕ when $m = 3$

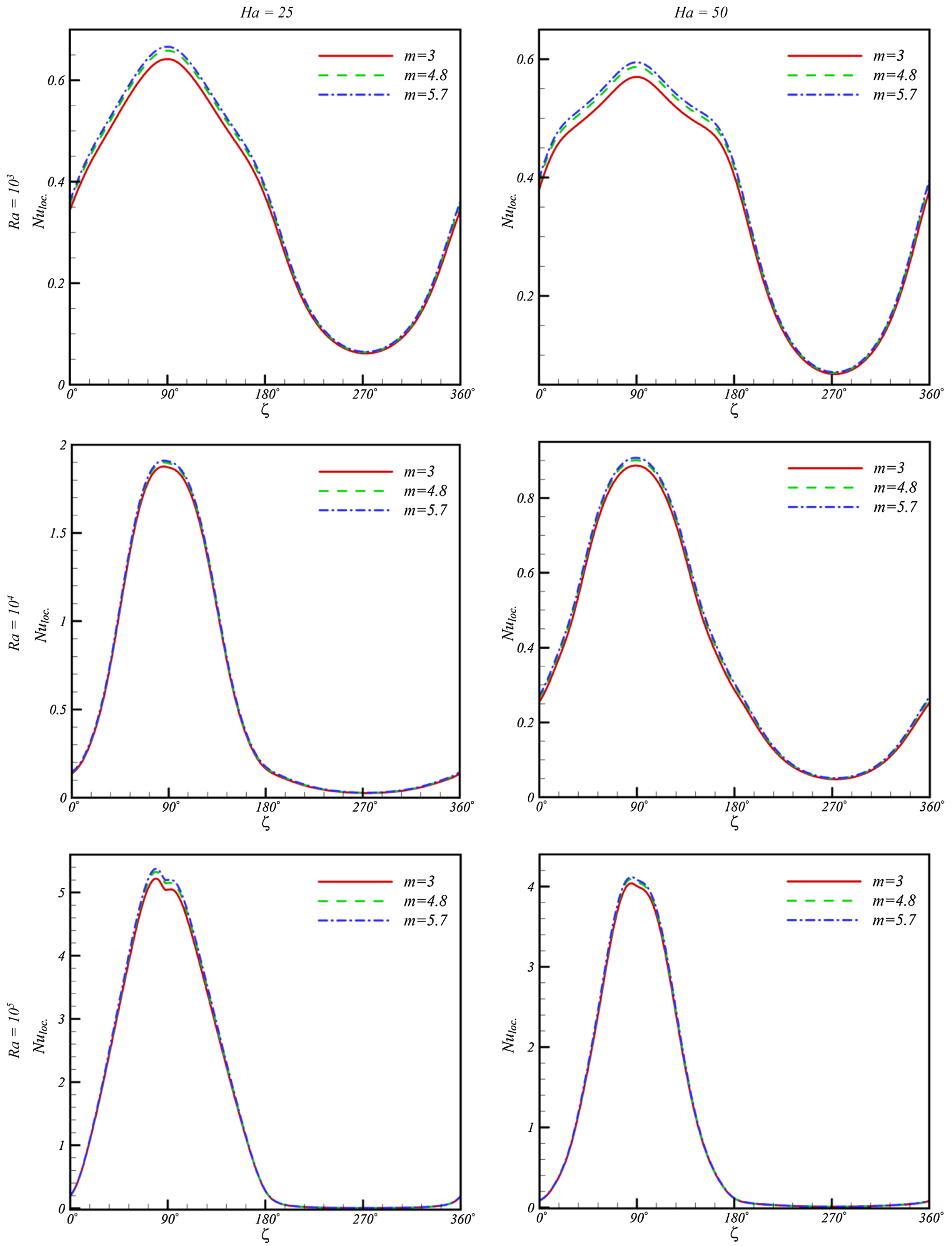

Fig. 7 Local Nusselt number ($Nu_{loc.}$) for different values of m at different conditions when $\phi = 2\%$

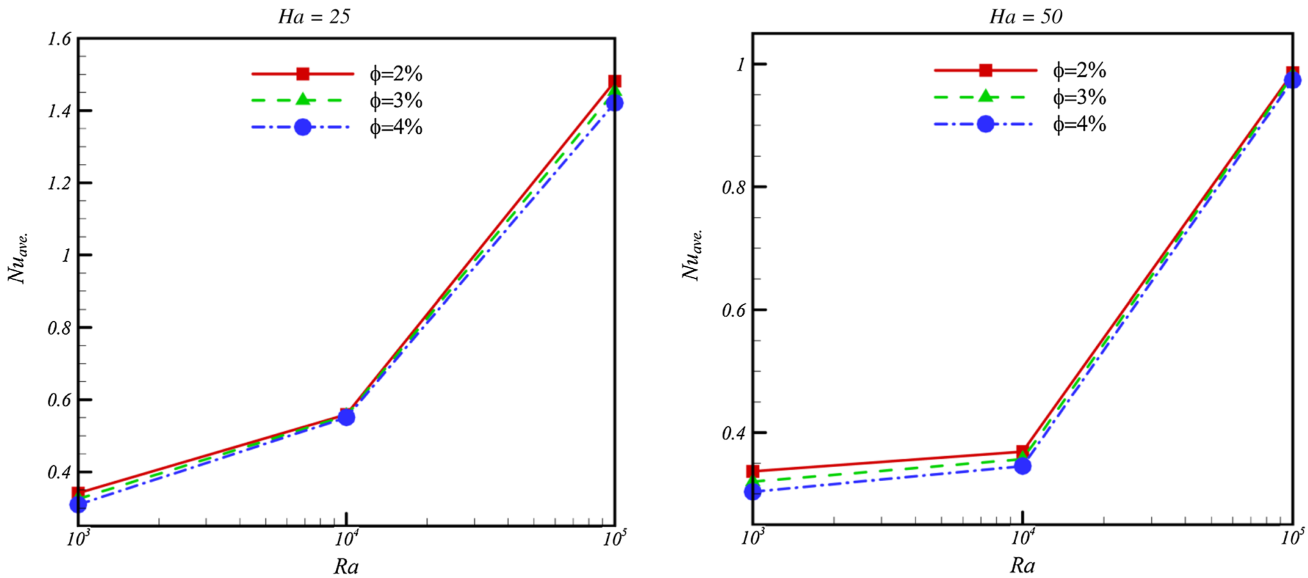

Fig. 8 Average Nusselt number ($Nu_{ave.}$) for different values of Ra, Ha and ϕ when $m=3$

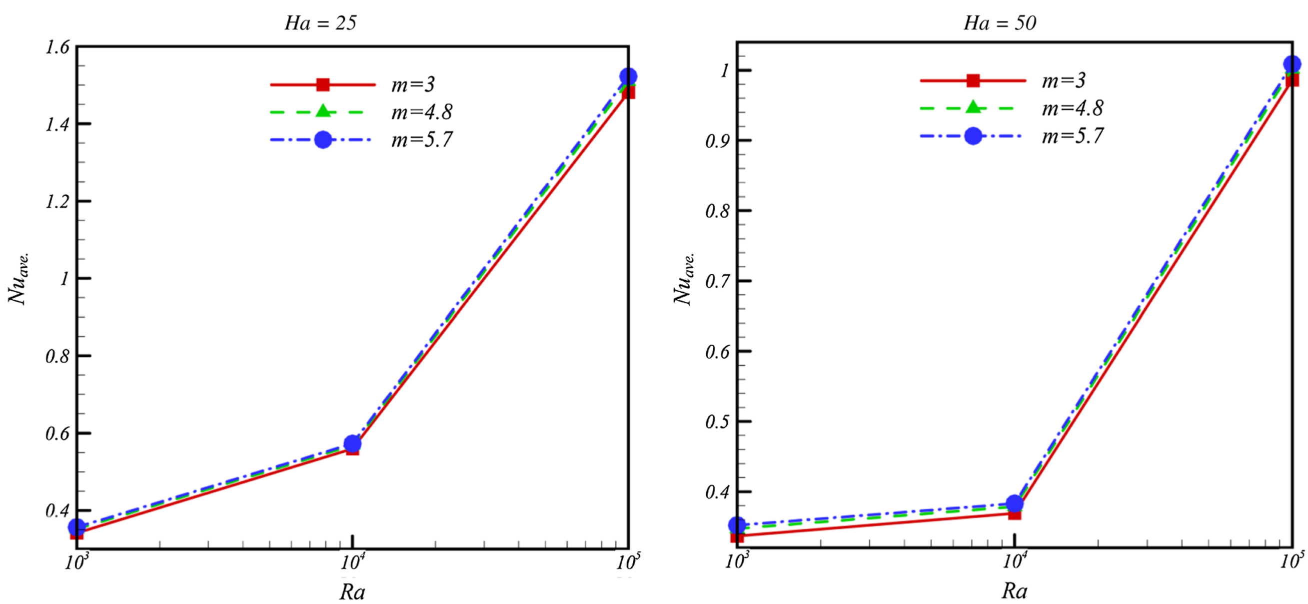

Fig. 9 Average Nusselt number ($Nu_{ave.}$) for different values of m at different conditions when $\phi = 2\%$

References

1. Eastman JA, Choi SUS, Li S, Yu W, Thompson LJ (2001) Anomalously increased effective thermal conductivities of ethylene glycol-based nano-fluids containing copper nanoparticles. Appl Phys Lett 78:718–720
2. Rajarathinam M, Nithyadevi N, Chamkha AJ (2017) Heat transfer enhancement of mixed convection in an inclined porous cavity using Cu–water nanofluid. Adv Powder Technol 29:590–605
3. Tiwari RK, Das MK (2007) Heat transfer augmentation in a two-sided lid-driven differentially heated square cavity utilizing nanofluids. Int J Heat Mass Transf 50:2002–2018

4. Iwatsu R, Hyun J, Kuwahara K (1993) Mixed convection in a driven cavity with a stable a stable vertical temperature gradient. Int J Heat Mass Transf 36:1601–1608
5. Mahdavi M, Sharifpur M, Ghodsinezhad H, Meyer JP (2016) Experimental and numerical study of the thermal and hydrodynamic characteristics of laminar natural convective flow inside a rectangular cavity with water, ethylene glycol–water and air. Exp Therm Fluid Sci 78:50–64
6. Koo J, Kleinstreuer C (2004) Viscous dissipation effects in micro tubes and micro channels. Int J Heat Mass Transf 47:3159–3169
7. Koo J (2004) Computational nanofluid flow and heat transfer analyses applied to microsystems. Ph.D thesis, NC State University, Raleigh, NC
8. Koo J, Kleinstreuer C (2005) Laminar nanofluid flow in microheat-sinks. Int J Heat Mass Transf 48:2652–2661
9. Dogonchi AS, Ganji DD (2016) Study of nanofluid flow and heat transfer between non-parallel stretching walls considering Brownian motion. J Taiwan Inst Chem Eng 69:1–3
10. Dogonchi AS, Ganji DD (2016) Thermal radiation effect on the nano-fluid buoyancy flow and heat transfer over a stretching sheet considering Brownian motion. J Mol Liq 223:521–527
11. Mastiani M, Kim MM, Nematollahi A (2017) Density maximum effects on mixed convection in a square lid-driven enclosure filled with Cu–water nanofluids. Adv Powder Technol 28:197–214
12. Mahapatra TR, Pal D, Mondal S (2013) Mixed convection flow in an inclined enclosure under magnetic field with thermal radiation and heat generation. Int Commun Heat Mass Transf 41:47–56
13. Dogonchi AS, Tayebi T, Chamkha AJ, Ganji DD (2019) Natural convection analysis in a square enclosure with a wavy circular heater under magnetic field and nanoparticles. J Therm Anal Calorim. https://doi.org/10.1007/s10973-019-08408-0
14. Dogonchi AS, Hashim (2019) Heat transfer by natural convection of Fe_3O_4–water nanofluid in an annulus between a wavy circular cylinder and a rhombus. Int J Heat Mass Transf 130:320–332
15. Seyyedi SM, Dogonchi AS, Nuraei R, Ganji DD, Hashemi-Tilehnoee M (2019) Numerical analysis of entropy generation of a nanofluid in a semi-annulus porous enclosure with different nanoparticle shapes in the presence of a magnetic field. Eur Phys J Plus 134:268. https://doi.org/10.1140/epjp/i2019-12623-1
16. Dogonchi AS, Waqas M, Seyyedi SM, Hashemi-Tilehnoee M, Ganji DD (2019) Numerical simulation for thermal radiation and porous medium characteristics in flow of CuO–H_2O nanofluid. J Braz Soc Mech Sci Eng 41:249. https://doi.org/10.1007/s40430-019-1752-5
17. Dogonchi AS, Waqas M, Ganji DD (2019) Shape effects of copper-oxide (CuO) nanoparticles to determine the heat transfer filled in a partially heated rhombus enclosure: CVFEM approach. Int Commun Heat Mass Transf 107:14–23
18. Dogonchi AS, Selimefendigil F, Ganji DD (2019) Magnetohydrodynamic natural convection of CuO–water nanofluid in complex shaped enclosure considering various nanoparticle shapes. Int J Numer Meth Heat Fluid Flow 29:1663–1679. https://doi.org/10.1108/HFF-06-2018-0294
19. Ghasemi E, Soleimani S, Bayat M (2013) Control volume based finite element method study of nano-fluid natural convection heat transfer in an enclosure between a circular and a sinusoidal cylinder. Int J Nonlinear Sci Numer Simul 14:521–532. https://doi.org/10.1515/ijnsns-2012-0177
20. Seyyedi SM, Dogonchi AS, Ganji DD, Hashemi-Tilehnoee M (2019) Entropy generation in a nanofluid-filled semi-annulus cavity by considering the shape of nanoparticles. J Therm Anal Calorim. https://doi.org/10.1007/s10973-019-08130-x
21. Ghasemi E, Soleimani S, Bararnia H (2012) Natural convection between a circular enclosure and an elliptic cylinder using control volume based finite element method. Int Commun Heat Mass Transfer 39:1035–1044
22. Seyyedi SM, Dogonchi AS, Hashemi-Tilehnoee M, Asghar Z, Waqas M, Ganji DD (2019) A computational framework for natural convective hydromagnetic flow via inclined cavity: an analysis subjected to entropy generation. J Mol Liq 287:110863. https://doi.org/10.1016/j.molliq.2019.04.140
23. Dogonchi AS, Armaghani T, Chamkha AJ, Ganji DD (2019) Natural convection analysis in a cavity with an inclined elliptical heater subject to shape factor of nanoparticles and magnetic field. Arab J Sci Eng. https://doi.org/10.1007/s13369-019-03956-x
24. Dogonchi AS, Chamkha AJ, Ganji DD (2019) A numerical investigation of magneto-hydrodynamic natural convection of Cu–water nanofluid in a wavy cavity using CVFEM. J Therm Anal Calorim 135:2599–2611
25. Khanafer K, Vafai K, Lightstone M (2003) Buoyancy-driven heat transfer enhancement in a two dimensional enclosure utilizing nanofluids. Int J Heat Mass Transf 46:3639–3653
26. De Vahl Davis G (1962) Natural convection of air in a square cavity, a benchmark numerical solution. Int J Numer Methods Fluids 3:249–264